Realistic shell-model calculations for *p*-shell nuclei including contributions of a chiral three-body force

T. Fukui,[1] L. De Angelis,[1] Y. Z. Ma,[2] L. Coraggio,[1] A. Gargano,[1] N. Itaco,[1,3] and F. R. Xu[2]

[1]*Istituto Nazionale di Fisica Nucleare, Complesso Universitario di Monte S. Angelo, Via Cintia, I-80126 Napoli, Italy*

[2]*School of Physics, and State Key Laboratory of Nuclear Physics and Technology, Peking University, Beijing I-100871, China*

[3]*Dipartimento di Matematica e Fisica, Università degli Studi della Campania "Luigi Vanvitelli," viale Abramo Lincoln 5 - I-81100 Caserta, Italy*

(Received 5 June 2018; published 5 October 2018)

In this paper we present an evolution of our derivation of the shell-model effective Hamiltonian, namely introducing effects of three-body contributions. More precisely, we consider a three-body potential at next-to-next-to-leading order in chiral perturbation theory, and the induced three-body forces that arise from many-body correlations among valence nucleons. The first one is included, in the derivation of the effective Hamiltonian for one- and two-valence nucleon-systems, at first order in the many-body perturbation theory. Namely, we include only the three-body interaction between one or two valence nucleons and those belonging to the core. For nuclei with more than two valence particles, both induced—turned on by the two-body potential—and genuine three-body forces come into play. Since it is difficult to perform shell-model calculations with three-body forces, these contributions are estimated for the ground-state energy only. To establish the reliability of our approximations, we focus attention on nuclei belonging to the *p* shell, aiming to benchmark our calculations against those performed with the *ab initio* no-core shell model. The obtained results are satisfactory, and pave the way to the application of our approach to nuclear systems with heavier masses.

DOI: 10.1103/PhysRevC.98.044305

I. INTRODUCTION

The shell model (SM) is a fundamental tool for the microscopic description of nuclear structure, and its most appealing feature is to reduce the complexity of a many-body problem, where the degrees of freedom of all the individual nucleons are explicitly taken into account, to the one where only the valence nucleons interact in a limited model space.

Within this framework, it is highly desirable to derive the SM parameters; namely, the single-particle (SP) energies and the two-body matrix elements (TBMEs) of the residual interaction from realistic nuclear forces. This approach is the so-called realistic shell model (RSM), and its roots trace back to the seminal paper by Kuo and Brown [1] more than fifty years ago, where a SM effective Hamiltonian $H_{\rm eff}$ for *sd*-shell nuclei was derived starting from the hard-core Hamada–Johnston potential [2]. Some historical developments of RSM may be found in review papers [3,4], and a certain number of fundamental papers on this topic are collected in Ref. [5].

Our approach to derive $H_{\rm eff}$ is based on the energy-independent linked-diagram perturbation theory [6], where the pivotal role is played by the perturbative expansion of the $\hat{Q}$-box vertex function, which is a collection of irreducible valence-linked Goldstone diagrams. The effective Hamiltonian is obtained by solving iteratively nonlinear matrix equations, that are expressed in terms of the $\hat{Q}$ box [7].

Recently, an alternative way to derive $H_{\rm eff}$, framed within a nonperturbative scheme, has been proposed [8]. This approach is an application of the in-medium similarity renormalization group [9] and may provide a new and valuable tool for the development of the RSM.

In a previous paper [10], we described in detail the process to derive $H_{\rm eff}$, and the procedures we apply to check both the convergence properties of the perturbative expansion and the weak dependence of the shell-model results upon the harmonic-oscillator (HO) parameter $\hbar\omega$. The latter dependence is introduced, as in all many-body techniques employing the HO auxiliary potential, by the truncation of the number of intermediate states in the sum of the perturbative expansion.

Moreover, to check the validity of our approach, we have performed benchmark calculations comparing the outcome of the diagonalization of RSM Hamiltonians with that of an *ab initio* method, such as the no-core shell model (NCSM) [11,12]. To this end, we derived *p*-shell effective Hamiltonians starting from a realistic nuclear potential based on the chiral perturbation theory (ChPT) at next-to-next-to-next-to-leading order (N^3LO) [13], but taking into account only the two-body ($2N$) component of this potential.

The comparison between the results obtained is very satisfactory, especially considering that, in NCSM, the degrees of freedom of all constituent nucleons are taken into account, while in RSM the eigenfunctions contain explicitly configurations of the valence nucleons only, which are constrained to a model space limited to the $0p_{3/2}$ and $0p_{1/2}$ orbitals.

As a matter of fact, the low-lying energy spectra of some *p*-shell nuclei calculated with RSM nicely agree with those by NCSM, while the discrepancy of the calculated ground-state energies, with respect to the ^{4}He core, grows with the mass number A. This can be explained by bearing in mind that our $H_{\rm eff}$ is derived for one- and two-valence-nucleon systems, while it neglects the many-body (>2) components of $H_{\rm eff}$, that

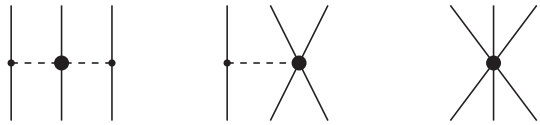

FIG. 1. The three-nucleon potential at N^{2}LO. From left to right: 2π-exchange, 1π-exchange, and contact diagrams.

arise from the interaction via the two-body force of the many-valence nucleons with core excitations as well as with virtual intermediate nucleons scattered above the model space.

In the present work, we address this issue by calculating the effect on the ground-state (g.s.) energies of three-body correlation diagrams [14,15], and also including in our $H_{\rm eff}$, aside the chiral N^{3}LO two-body potential [13,16], a chiral next-to-next-to-leading order (N^{2}LO) three-body potential [12] whose effects are considered at first order in perturbation theory.

So far, modern nuclear structure calculations have evidenced the role played by three-nucleon ($3N$) forces, in particular for light nuclei with $A \leqslant 12$ (see, for example, Refs. [17,18]). Our goal is to obtain an improvement of the reproduction of the spectroscopic properties of p-shell nuclei, and benchmark our results against those in Refs. [12,19], by including the same chiral three-body potential.

It is worth mentioning that our approach to treat the microscopic $3N$ potential is similar to that in Refs. [20–23] where, aside a realistic two-body low-momentum potential, only first-order contributions of the normal-ordered two-body parts of $3N$ forces have been taken explicitly into account.

The paper is organized as follows: In Sec. II we give an outline of the derivation of our shell-model effective Hamiltonian within a perturbative approach, and of our procedure to include three-body effects. Section III is devoted to compare our RSM results with those provided by the *ab initio* NCSM [12,19]. Concluding remarks and outlook of our future commitments are given in Sec. IV. In the Appendix, details of the calculations of the matrix elements of the N^{2}LO three-body potential are reported.

II. THEORETICAL FRAMEWORK

As mentioned in the introduction, a detailed description of the procedure we apply to derive $H_{\rm eff}$ within the many-body perturbation theory has been reported in Ref. [10].

We start our calculations by considering a high-precision nucleon-nucleon (NN) potential derived within the ChPT at next-to-next-to-next-to-leading order [13,16]. In the chiral perturbative expansion the $3N$ potentials appear from N^{2}LO on, and we consider also its contributions in the derivation of the $H_{\rm eff}$.

This $3N$ potential consists of three components (see Fig. 1); namely, the two-pion (2π) exchange term $V_{3N}^{(2\pi)}$, the one-pion (1π) exchange plus contact term $V_{3N}^{(1\pi)}$, and the contact term $V_{3N}^{(\rm ct)}$.

It should be pointed out that the low-energy constants (LECs) c_1, c_3, and c_4, appearing in $V_{3N}^{(2\pi)}$ are the same as those in the NN potential, so their values are fixed by the renormalization procedure that is performed for the two-body N^{3}LO potential [16]. However, the $3N$ 1π-exchange term and the contact interaction are characterized by two extra LECs (known as c_D and c_E, respectively), which cannot be constrained by two-body observables, and need to be fit in order to reproduce observables in systems with mass $A > 2$.

Since we intend to benchmark our SM calculations against those in Refs. [12,19], in this work we adopt $c_D = -1$, as reported in Ref. [12], and $c_E = -0.34$, as may be inferred from Fig. 1 in the same reference.

The N^{2}LO $3N$ potential is defined in momentum space and, in order to employ it to derive a shell-model effective interaction, we have calculated its matrix elements in the HO basis following a procedure similar to that indicated in Ref. [24]. Actually, there is a difference about the calculation of the two-pion exchange term with our formalism and the one reported in Ref. [24], and the details of our calculations are reported in the Appendix.

Note that the Coulomb potential is explicitly taken into account in our calculations.

After choosing the NN and $3N$ potentials, our next step is to derive a SM effective Hamiltonian for one- and two-valence-nucleon systems within a model space spanned by the two proton and neutron orbitals $0p_{3/2}$ and $0p_{1/2}$, outside the doubly closed ^{4}He core.

To this end, an auxiliary one-body potential U is introduced in order to break up the intrinsic Hamiltonian for a system of A nucleons as the sum of a one-body term H_0, which describes the independent motion of the nucleons, and a residual interaction H_1:

$$\begin{aligned} H_{\rm int} &= \left(1-\frac{1}{A}\right)\sum_i \frac{p_i^2}{2m} \\ &\quad + \sum_{i<j}\left(V_{ij}^{NN} - \frac{\mathbf{p_i}\cdot\mathbf{p_j}}{mA}\right) + \sum_{i<j<k} V_{ijk}^{3N} \\ &= \sum_i \left(\frac{p_i^2}{2m} + U_i\right) \\ &\quad + \sum_{i<j}\left(V_{ij}^{NN} - U_i - \frac{p_i^2}{2mA} - \frac{\mathbf{p_i}\cdot\mathbf{p_j}}{mA}\right) + \sum_{i<j<k} V_{ijk}^{3N} \\ &= H_0 + H_1, \end{aligned} \tag{1}$$

where i, j, k indices run from 1 to the mass number A, and $\mathbf{p}$ is the momentum of the nucleon. Note that, in order to compare RSM with NCSM results, we have to employ a purely intrinsic Hamiltonian by removing the center-of-mass (c.m.) kinetic energy. This introduces a dependence on the mass number A that is relevant for light systems, such as those belonging to the p shell, but that is strongly suppressed for heavier nuclei.

The diagonalization of the many-body Hamiltonian $H_{\rm int}$ in an infinite Hilbert space is unfeasible, and our eigenvalue problem is then reduced to the one for an effective Hamiltonian $H_{\rm eff}$ in a truncated model space. Since $H_{\rm int}$ has been broken up into two terms, we define the reduced model space in terms of a finite subset of H_0 eigenvectors. In our calculation we choose as auxiliary potential U the HO potential.

In this paper, we resort to the Kuo–Lee–Ratcliff (KLR) folded-diagram expansion [6,25] to calculate $H_{\rm eff}$, and this can be done by way of a perturbative expansion of the vertex function $\hat{Q}$ box:

$$\hat{Q}(\epsilon) = PH_1P + PH_1Q\frac{1}{\epsilon - QHQ}QH_1P, \qquad (2)$$

as defined in Ref. [7].

In our calculations we expand the $\hat{Q}$ box in terms of irreducible valence-linked one- and two-body Goldstone diagrams through third order in H_1, for contributions with $2N$ vertices [10], and up to first order for those with a $3N$ vertex. Then, to have a better estimate of the value to which the perturbation series should converge, we resort to the Padé approximant theory [26,27], and calculate the Padé approximant [2|1] of the $\hat{Q}$ box, as suggested in Ref. [28]:

$$[2|1] = V^0_{\rm Qbox} + V^1_{\rm Qbox} + V^2_{\rm Qbox}\left[1 - \left(V^2_{\rm Qbox}\right)^{-1}V^3_{\rm Qbox}\right]^{-1}. \quad (3)$$

$V^n_{\rm Qbox}$ is the square nonsingular matrix representing the nth-order contribution to the $\hat{Q}$ box in the perturbative expansion.

We have reviewed the calculation of our SM effective Hamiltonian $H_{\rm eff}$ in Ref. [10], where details of the diagrammatic expansion of the $\hat{Q}$ box and its perturbative properties are also reported.

In terms of the $\hat{Q}$ box, the SM effective Hamiltonian can be written in an operator form as

$$H_{\rm eff} = \hat{Q} - \hat{Q}'\int\hat{Q} + \hat{Q}'\int\hat{Q}\int\hat{Q} - \hat{Q}'\int\hat{Q}\int\hat{Q}\int\hat{Q} + \cdots, \qquad (4)$$

where the integral sign represents a generalized folding operation, and $\hat{Q}'$ is obtained from $\hat{Q}$ by removing terms at the first order in the NN potential [6,25]. The folded-diagram series is then summed up to all orders by using the Lee–Suzuki iteration method [7].

In Ref. [10] the values of the SP energies and TBME derived including only the N^{3}LO two-body force have been reported.

As shown in the above paper, the diagonalization of $H_{\rm eff}$ performed for some p-shell nuclei, such as ^{6}Li and ^{10}B, provides excitation spectra that are in a close agreement with those obtained in NCSM calculations starting from the same N^{3}LO two-body potential [12,19].

As regards the calculated g.s. energies, with respect to the ^{4}He core, the agreement between RSM and NCSM deteriorates when increasing the number of valence nucleons in the shell-model calculations. This may be ascribed to the fact that our SM Hamiltonian is derived just for one- and two-valence-nucleon systems and, as mentioned in the introduction, for nuclei with more valence nucleons, the $\hat{Q}$ box should contain diagrams with at least three incoming and outcoming valence particles. The leading terms of such correlation diagrams appear at second order in perturbation theory for three-valence-nucleon systems and are reported in Fig. 2.

The explicit expressions of these three-body diagrams are reported in Ref. [15]. Since the inclusion of a three-body term in the shell-model Hamiltonian cannot be managed by the SM code we employ [29], we calculate the contribution of the monopole component of the three-body diagrams and add it to the calculated g.s. energies.

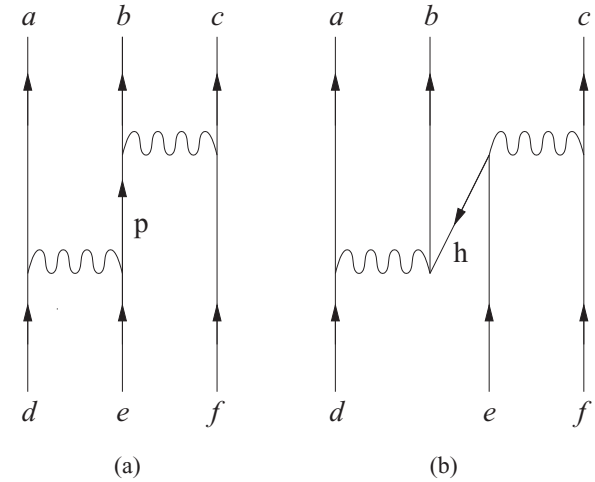

FIG. 2. Second-order three-body diagrams. The sum over the intermediate lines runs over particle and hole states outside the model space, shown by A and B, respectively. For the sake of simplicity, for each topology we report only one of the diagrams which correspond to the permutations of the external lines.

As already mentioned in the introduction, we calculate $H_{\rm eff}$ introducing also the contributions of a N^{2}LO $3N$ potential. More precisely, we evaluate its contribution at first order in many-body perturbation theory only for the one- and two-valence-nucleon systems.

As regards the contribution to the single-particle component of the $\hat{Q}$ box from a three-body potential we report in Fig. 3 the diagram at first order, whose explicit expression is

$$\langle j_a|1\mathrm{b}_{3N}|j_a\rangle = \sum_{\substack{h_1,h_2\\J_{12}J}}\frac{\hat{J}^2}{2\hat{j}_a^{\,2}}\langle\left[\left(j_{h_1}j_{h_2}\right)_{J_{12}},j_a\right]_J|\times V_{3N}|\left[\left(j_{h_1}j_{h_2}\right)_{J_{12}},j_a\right]_J\rangle. \qquad (5)$$

The expression of the first-order two-body diagram with a $3N$ vertex, shown in Fig. 3, is the following:

$$\langle(j_aj_b)_J|2\mathrm{b}_{3N}|(j_cj_d)_J\rangle = \sum_{h,J'}\frac{\hat{J}'^2}{\hat{J}^2}\langle[(j_aj_b)_J,j_h]_{J'}|V_{3N}|[(j_cj_d)_J,j_h]_{J'}\rangle, \qquad (6)$$

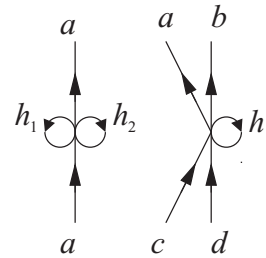

FIG. 3. First-order one- and two-body diagrams with a three-body-force vertex. See text for details.

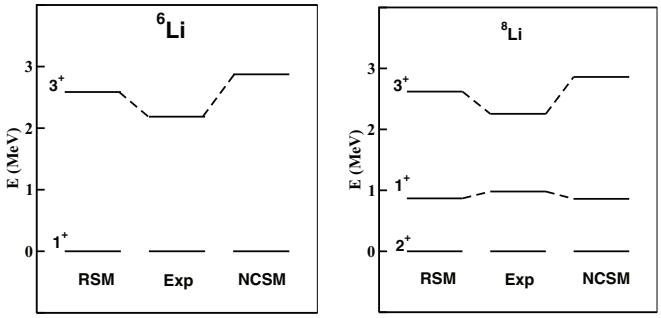

FIG. 4. Low-lying energy spectra of ^{6}Li and ^{8}Li. In the middle the experimental levels are given, and the calculated ones (starting from a two-body potential only) with RSM and NCSM are reported on the left and the right sides of the figure, respectively.

The three-body matrix element (3BME) $\langle[(j_a j_b)_{J_{ab}}, j_c]_J | V_{3N} | [(j_d j_e)_{J_{de}}, j_f]_J \rangle$, expressed within the proton-neutron formalism, is antisymmetrized but not normalized.

It is worth mentioning that the expressions in Eqs. (5) and (6) are the coefficients which multiply the one- and two-body terms, respectively, arising from the normal-ordering decomposition of the three-body component of a many-body Hamiltonian [30].

In the Supplemental Material [31], the calculated SP energies and TBME of our SM Hamiltonians for $A = 6$, 8, 10, and 12 can be found. As pointed out in Ref. [10], the A dependence of our $H_{\rm eff}$s, due to Eq. (1), affects mostly the calculated g.s. energies and very weakly the excited spectra.

III. RESULTS

In the following sections, the results of our shell-model calculations are presented: first those obtained starting from the N^{3}LO NN potential only, and then those including also the contributions of the N^{2}LO $3N$ potential. The calculated spectra and binding energies are compared with those reported in Refs. [12,19], in order to benchmark our approach against NCSM, and with the corresponding experimental data.

A. Calculations with NN potential

In Figs. 4–7, the low-energy spectra of ^{6}Li, ^{8}Li, ^{8}B, ^{8}Be, ^{10}B, ^{11}B, ^{12}C, and ^{13}C, calculated in our RSM framework, are compared with the experimental ones [32] and those obtained with NCSM [12,19]. From the inspection of Figs. 4–7, it can be seen that there is an excellent agreement between RSM and NCSM, especially for low energy levels.

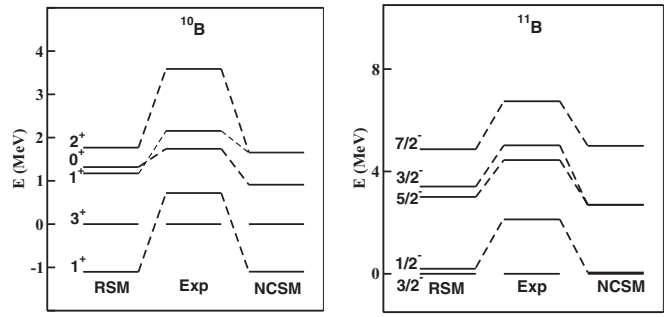

FIG. 6. Same as Fig. 4, but for ^{10}B and ^{11}B.

In Fig. 6, we see that both RSM and NCSM predict the inversion of the $J^\pi = 3^+$ g.s. and the first-excited $J^\pi = 1^+$ state in ^{10}B. This defect is healed, as we will see in the next section, by including the $3N$-potential contributions.

As regards ^{11}B, both RSM and NCSM calculations provide two low-lying doublets; the almost-degenerate $J^\pi = (\frac{1}{2}^-)_1$, $(\frac{3}{2}^-)_1$ and $J^\pi = (\frac{3}{2}^-)_2$, $(\frac{5}{2}^-)_1$ states. There is no experimental counterpart of these degeneracies, which will be removed including the contribution of a $3N$ potential.

In Fig. 7 we report the first-excited states of ^{12,13}C isotopes. It can be seen that both RSM and NCSM fail to reproduce the observed excitation energy of the yrast $J^\pi = 2^+$ state in ^{12}C, which is underestimated by $\sim$1 MeV.

In Fig. 15 of Ref. [10] we compared our calculated g.s. energies with respect to ^{4}He of $N = Z$ nuclei—up to ^{12}C—with those of NCSM calculations [12,19]. Our calculated energies were increasingly underbinding, with respect to the NCSM ones, and in Ref. [10] we have ascribed this defect to the lack of many-body components of our $H_{\rm eff}$, whose role should grow with the number of valence nucleons.

As mentioned in Sec. II, we can now include the three-body diagrams in Fig. 2 by calculating their monopole components and then adding their contributions to the calculated g.s. energies. The results of this procedure are reported in Fig. 8, where the new calculated RSM g.s. energies (black diamonds) are compared with both the experimental ones (red triangles) and those obtained with NCSM (blue bullets). As can be seen,

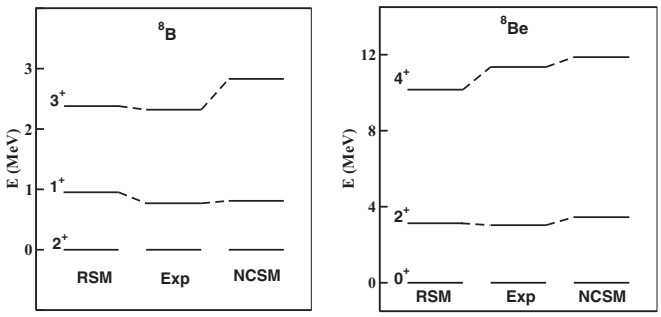

FIG. 5. Same as Fig. 4, but for ^{8}B and ^{8}Be.

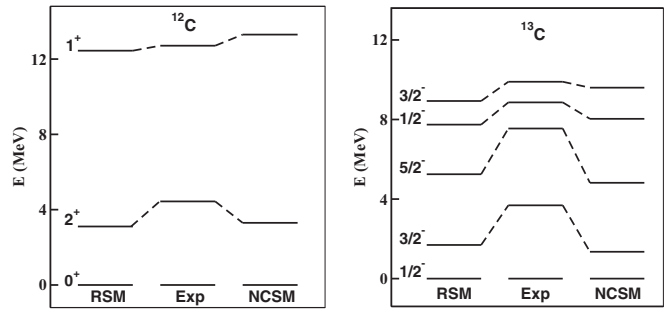

FIG. 7. Same as Fig. 4, but for ^{12}C and ^{13}C.

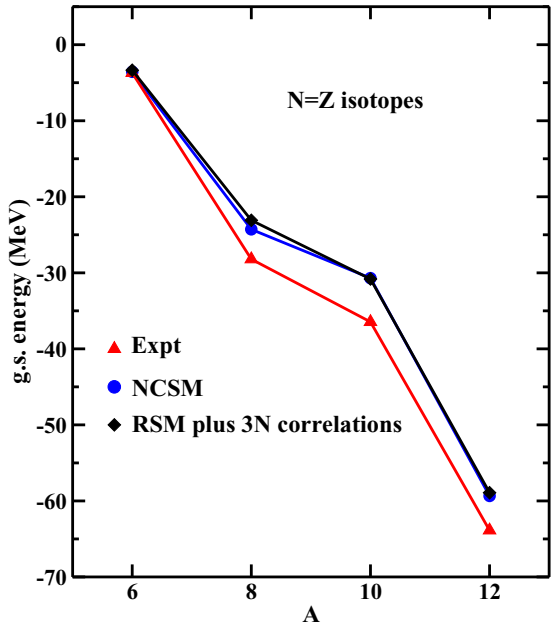

FIG. 8. Ground-state energies for $N = Z$ nuclei with mass $6 \leqslant A \leqslant 12$.

we have efficiently improved the comparison between RSM and NCSM, the largest discrepancy being about 4% for ^{8}Be.

B. Calculations with NN plus $3N$ potentials

In Figs. 9–12, we show the low-energy spectra of ^{6}Li, ^{8}Li, ^{8}B, ^{8}Be, ^{10}B, ^{11}B, ^{12}C, and ^{13}C, calculated in our RSM framework, now including also the contributions from the N^{2}LO $3N$ potential as reported in Sec. II. We compare them with the experimental ones [32] and the NCSM results [12,19].

As in the case with only N^{3}LO NN potential, our results and the NCSM ones are in close agreement. Moreover, the theory with $3N$ compares far better with experiment, as can be seen in all the reported spectra.

In particular, the experimental sequence of observed states in ^{10}B is restored, and the degeneracies of $J^\pi = (\frac{1}{2}^-)_1$, $(\frac{3}{2}^-)_1$ and $J^\pi = (\frac{3}{2}^-)_2$, $(\frac{5}{2}^-)_1$ states in ^{11}B is removed. This supports

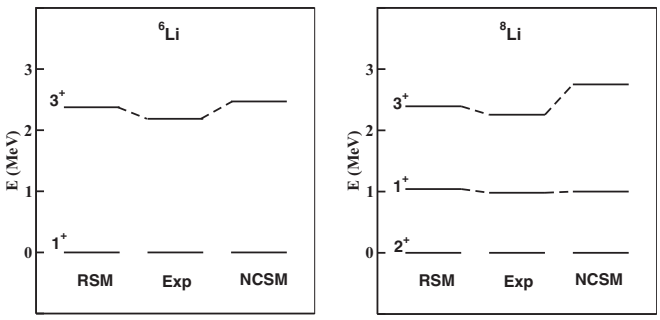

FIG. 9. Same as Fig. 4 except that both RSM and NCSM include the N^{2}LO $3N$ potential.

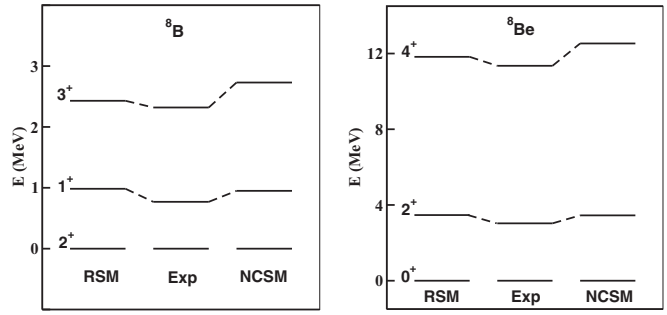

FIG. 10. Same as Fig. 9, but for ^{8}B and ^{8}Be.

the crucial role played by the $3N$ potential to improve the spectroscopic description of p-shell nuclei.

We recall here that the effective single-particle energies (ESPEs) are related to the monopole part of the shell-model Hamiltonian, thus reflecting the angular-momentum-averaged effects of the shell-model interaction $V^{\rm SM}$ for a given nucleus. The ESPE of a level is defined as the one-neutron separation energy of this level, and calculated in terms of the bare ϵ_j and the monopole part of the interaction; namely, $\mathrm{ESPE}(j) = \epsilon_j + \sum_{j'} V^{\rm SM}_{jj'} n_{j'}$, where the sum runs on the model-space levels j', n_j being the number of particles in the level j and $V^{\rm SM}_{jj'}$ the angular-momentum-averaged interaction $V^{\rm SM}_{jj'} = \sum_J (2J+1)\langle jj'|V^{\rm SM}|jj'\rangle_J / \sum_J (2J+1)$.

In Figs. 13 and 14, we show the evolution of proton and neutron $0p_{1/2}$ ESPE relative to $0p_{3/2}$, respectively, as a function of A for $N = Z$ isotopes.

The behavior of proton and neutron ESPEs is helpful to understand the different properties of $H_{\rm eff}$, including or not contributions of the N^{2}LO $3N$ potential. As can be seen in Figs. 13 and 14, the relative ESPE rapidly drops down when considering only the N^{3}LO NN potential, even becoming negative around $A = 8$. Actually, the relative ESPE is almost constant when the $3N$ potential is taken into account, being $4 \sim 5$ MeV.

This reflects in the calculated energy spacings between yrast $J^\pi = \frac{1}{2}^-$ and $\frac{3}{2}^-$ in ^{11}B and, more important in the higher excitation energy of the yrast $J^\pi = 2^+$ state in ^{12}C spectra reported in Figs. 7 and 12. In fact, calculations including the three-body force lead to a better comparison with experiment.

It is worth pointing out that many studies have been performed about the crucial role played by three-body potentials

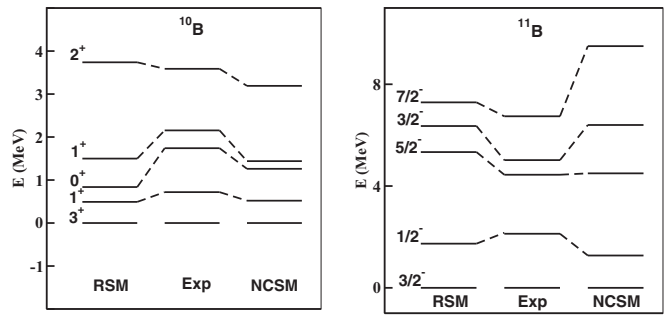

FIG. 11. Same as Fig. 9, but for ^{10}B and ^{11}B.

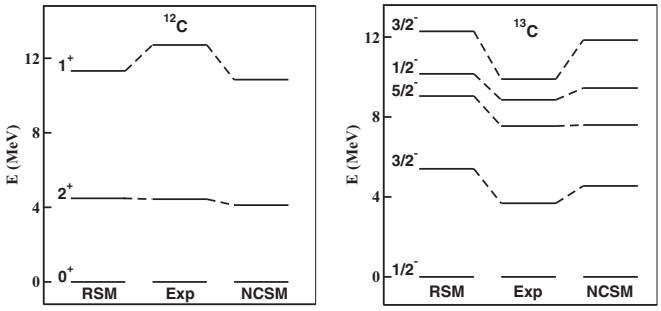

FIG. 12. Same as Fig. 9, but for ^{12}C and ^{13}C.

on the monopole properties of SM effective interactions (see, for instance, Refs. [33,34]), especially to obtain the correct shell-closure properties when starting from realistic forces. Recent progress in SM calculations, including three-body force effects [20,35], has proven the validity of such a speculation, and our results support the prospect that a consistent derivation of $H_{\rm eff}$ from chiral two- and three-body potentials may lead to an improvement of the theoretical description of nuclear systems with larger mass number A.

For the sake of completeness, in Fig. 15 we report the g.s. energies of $N = Z$ isotopes, that, as in Fig. 8, have been obtained by taking into account also $3N$ correlations. Namely, we add to the energies calculated with $H_{\rm eff}$, now including a N^{2}LO $3N$ potential, only the contribution of their monopole component. It is worth pointing out that the results with RSM are not satisfactory. Actually, there is a substantial discrepancy between results obtained with RSM and those calculated with NCSM, since our RSM calculations underestimate the contribution of the $3N$ potential. This may be mainly ascribed to the fact that, at present, our $H_{\rm eff}$ includes only first-order contributions.

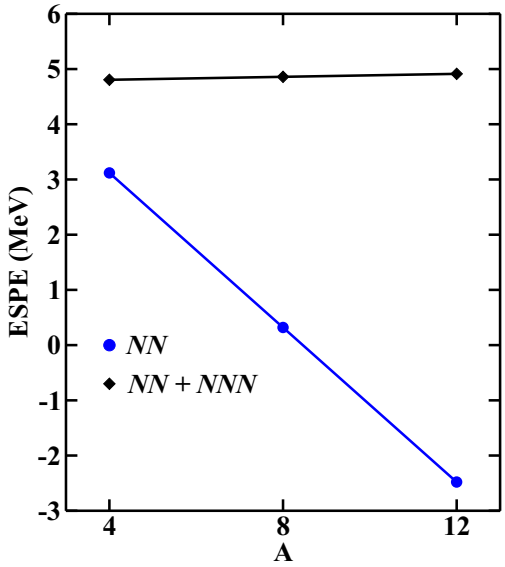

FIG. 13. Proton $0p_{1/2}$ ESPE relative to $0p_{3/2}$ as a function of A (see text for details). The diamond and bullet symbols refer to results obtained with and without $3N$ contributions, respectively.

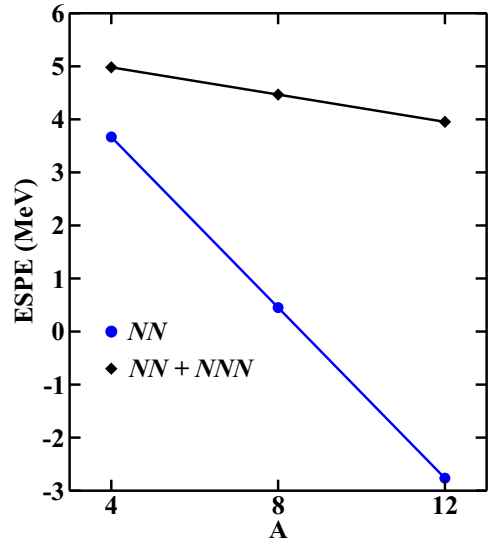

FIG. 14. Same as in Fig. 13, but for neutron ESPE.

IV. CONCLUDING REMARKS AND OUTLOOK

In this paper we have presented the results that we have obtained for p-shell nuclei in the framework of RSM, taking into account the contributions of both induced and genuine three-body forces.

On one side, we have shown how the inclusion of the three-body correlations between valence nucleons that are induced by the NN potential due to the truncation of the Hilbert space greatly improves the agreement of our calculated binding energies with respect to those obtained by *ab initio* calculations.

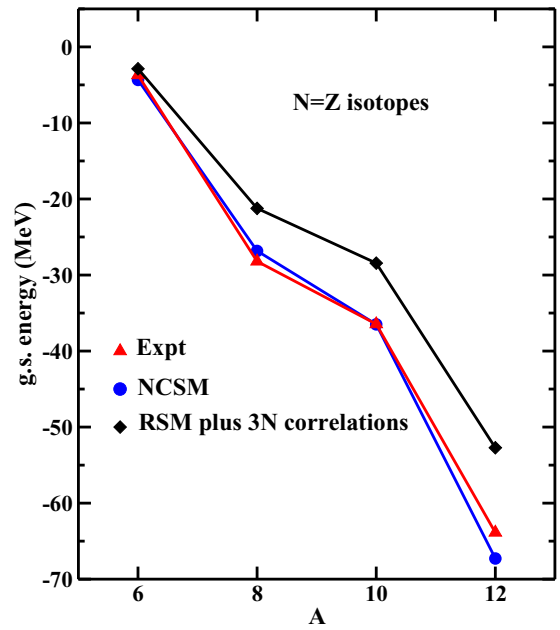

FIG. 15. Same as Fig. 8, but including also contributions of N^{2}LO $3N$ potential both in RSM and NCSM calculations.

On the other side, we have calculated the contribution at first order in perturbation theory of a N^{2}LO chiral $3N$ potential to the SM effective Hamiltonian, and the comparison of our calculated energy spectra with those from NCSM [12,19] turns out to be successful, thus supporting the reliability of RSM calculations.

Actually, as reported in Sec. III B, our g.s. energies—calculated including the N^{2}LO $3N$ potential—reflect the lack of higher-order contributions to the perturbative expansion of $H_{\rm eff}$. This is evidenced by the underestimation of the binding energies obtained with NCSM; the latter reproducing satisfactorily the observed ones.

In this regard, the next step of our study will be to include higher-order contributions with $3N$ vertices in the perturbative expansion of the $\hat{Q}$ box, in order to establish their role in the evolution of the spectroscopic properties provided by RSM.

ACKNOWLEDGMENTS

This work has been supported by the Natural Science Foundation of China under Grants No. 11320101004 and No. 11575007; and the CUSTIPEN (China-U.S. Theory Institute for Physics with Exotic Nuclei) funded by the US Department of Energy, Office of Science under Grant No. DE-SC0009971. The authors thank P. Navrátil, G. De Gregorio, and T. Miyagi for helpful comments and fruitful discussions. The calculations have been carried out at MARCONI of CINECA, Italy.

APPENDIX: CALCULATION OF THREE-BODY MATRIX ELEMENTS

Our aim is to calculate the three-body matrix elements of the chiral potential at N^{2}LO between the antisymmetrized three-particle HO states. To this end, we follow the procedure sketched below:

(i) Transformation of the JT-coupled three-particle HO basis into the Jacobi-HO basis, thus separating the c.m. and relative motions;
(ii) antisymmetrization of the Jacobi-HO basis;
(iii) evaluation of the Jacobi-HO matrix element (ME), which is the 3BME of the chiral interaction at N^{2}LO [16,36].

Our approach to steps (i) and (ii) is essentially same as that used in Ref. [24].

The transformation in step (i) leads to the so-called T coefficients (see, for instance, Ref. [37]), involving angular-momentum recouplings and the HO brackets originating from the Talmi transformation [38–42]. The HO brackets are computed by using the Fortran code of Ref. [43].

At the step (ii), as suggested in Refs. [44,45], we build up the antisymmetrized Jacobi-HO states $|\kappa; JT\rangle_A$ by diagonalizing the three-body antisymmetrizer. Thus we obtain

$$|\kappa; JT\rangle_A = \sqrt{6}\sum_{\bar{\kappa}} D^{(JT)}_{\kappa\bar{\kappa}}\,|\bar{\kappa}; JT\rangle\,, \tag{A1}$$

$$D^{(JT)}_{\kappa\bar{\kappa}} = \sum_{\eta}\langle\kappa; JT\,|\,\eta\rangle\langle\eta\,|\,\bar{\kappa}; JT\rangle, \tag{A2}$$

where $|\eta\rangle$ is a "physical" eigenstate [45] of the three-body antisymmetrizer, and it corresponds to the eigenvalue 1. The index κ for the totally antisymmetrized Jacobi-HO states $|\kappa; JT\rangle_A$ stands for the set of the quantum numbers $\{n_{12}, l_{12}, S_{12}, I_{12}, T_{12}, n, l, I\}$. The quantum numbers with the subscript "12" are associated with the a-b system; that is, the principal quantum number n_{12}, the orbital angular momentum l_{12}, the two-nucleon coupled spin S_{12}, the angular momentum I_{12} originating from the coupling of l_{12} and S_{12}, and the two-nucleon coupled isospin T_{12}. Whereas the (ab)-c motion is characterized by the principal quantum number n, the orbital angular momentum l, and the angular momentum I coming from the coupling of l and the nucleon spin $1/2$. The total angular momentum J (isospin T) is formed by the coupling of I_{12} and I (T_{12} and nucleon isospin $1/2$). The index $\bar{\kappa} = \{\bar{n}_{12}, \bar{l}_{12}, \bar{S}_{12}, \bar{I}_{12}, \bar{T}_{12}, \bar{n}, \bar{l}, \bar{I}\}$ is similar to κ but for the Jacobi-HO states $|\bar{\kappa}; JT\rangle$, which is partially antisymmetrized with respect to the a-b system with the constraint $(-1)^{\bar{l}_{12}+\bar{S}_{12}+\bar{T}_{12}} = -1$.

As regards the step (iii), the Jacobi-HO MEs both of the one-pion-exchange plus-contact operator $V^{(1\pi)}_{3N}$ and the $3N$ contact operator $V^{(\rm ct)}_{3N}$ are evaluated with a nonlocal regulator [see Eq. (A8)] following the procedure described in Ref. [24]. At variance with Ref. [24], the Jacobi-HO ME of the two-pion exchange operator $V^{(2\pi)}_{3N}$ is calculated in an alternative way explained below.

Owing to Eq. (A1) and the symmetry of $V^{(2\pi)}_{3N}$ with respect to the permutation of particles, the antisymmetrized Jacobi-HO ME is given by

$${}_A\langle\kappa'; JT|V^{(2\pi)}_{3N}|\kappa; JT\rangle_A = 18\sum_{\bar{\kappa}\bar{\kappa}'} D^{(JT)}_{\kappa\bar{\kappa}} D^{(JT)}_{\kappa'\bar{\kappa}'}\langle\bar{\kappa}'; JT|\left[W^{(2\pi;c_1)}_{3N} + W^{(2\pi;c_3)}_{3N} + W^{(2\pi;c_4)}_{3N}\right]|\bar{\kappa}; JT\rangle, \tag{A3}$$

The momentum representation of the reduced operator $W^{(2\pi;c_\mu)}_{3N}$, with $\mu = 1$, 3, or 4, is written as

$$\langle \boldsymbol{p}'_a\boldsymbol{p}'_b\boldsymbol{p}'_c|W^{(2\pi;c_\mu)}_{3N}|\boldsymbol{p}_a\boldsymbol{p}_b\boldsymbol{p}_c\rangle = w^{(2\pi;c_\mu)}_{3N}(\boldsymbol{q}_b, \boldsymbol{q}_c)\delta(\boldsymbol{q}_a + \boldsymbol{q}_b + \boldsymbol{q}_c). \tag{A4}$$

Here, for convenience, we define $w_{3N}^{(2\pi;c_\mu)}$ as a function of $\boldsymbol{q}_b$ and $\boldsymbol{q}_c$, because these two transferred momenta are simply written in terms of the Jacobi momenta we employ [see Eq. (A9)]. The explicit form of $w_{3N}^{(2\pi;c_\mu)}$ is expressed as follows (see, for example, Refs. [16,46]):

$$w_{3N}^{(2\pi;c_1)}(\boldsymbol{q}_b,\boldsymbol{q}_c)=-\frac{1}{(2\pi)^6}\frac{g_A^2 c_1 m_\pi^2}{f_\pi^4}\frac{(\boldsymbol{\sigma}_b\cdot\boldsymbol{q}_b)(\boldsymbol{\sigma}_c\cdot\boldsymbol{q}_c)}{\left(q_b^2+m_\pi^2\right)\left(q_c^2+m_\pi^2\right)}\boldsymbol{\tau}_b\cdot\boldsymbol{\tau}_c, \tag{A5}$$

$$w_{3N}^{(2\pi;c_3)}(\boldsymbol{q}_b,\boldsymbol{q}_c)=\frac{1}{(2\pi)^6}\frac{g_A^2 c_3}{2f_\pi^4}\frac{(\boldsymbol{\sigma}_b\cdot\boldsymbol{q}_b)(\boldsymbol{\sigma}_c\cdot\boldsymbol{q}_c)}{\left(q_b^2+m_\pi^2\right)\left(q_c^2+m_\pi^2\right)}(\boldsymbol{q}_b\cdot\boldsymbol{q}_c)(\boldsymbol{\tau}_b\cdot\boldsymbol{\tau}_c), \tag{A6}$$

$$w_{3N}^{(2\pi;c_4)}(\boldsymbol{q}_b,\boldsymbol{q}_c)=\frac{1}{(2\pi)^6}\frac{g_A^2 c_4}{4f_\pi^4}\frac{(\boldsymbol{\sigma}_b\cdot\boldsymbol{q}_b)(\boldsymbol{\sigma}_c\cdot\boldsymbol{q}_c)}{\left(q_b^2+m_\pi^2\right)\left(q_c^2+m_\pi^2\right)}\{(\boldsymbol{q}_b\times\boldsymbol{q}_c)\cdot\boldsymbol{\sigma}_a\}\{(\boldsymbol{\tau}_b\times\boldsymbol{\tau}_c)\cdot\boldsymbol{\tau}_a\}, \tag{A7}$$

where $\boldsymbol{\sigma}_i$ ($\boldsymbol{\tau}_i$) is the Pauli spin (isospin) matrix of nucleon i ($i=a$, b, or c), and the transferred momentum is $\boldsymbol{q}_i=\boldsymbol{p}_i'-\boldsymbol{p}_i$, with $\boldsymbol{p}_i$ and $\boldsymbol{p}_i'$ being the initial and final momenta, respectively. We use the parameters, $g_A=1.29$, $f_\pi=92.4$ MeV, $m_\pi=138.04$ MeV, and $\Lambda_\chi=700$ MeV. In this paper the parameters are given in natural units; namely, $c=\hbar=1$. Note that, in $w_{3N}^{(2\pi;c_\mu)}$ there is a prefactor $1/(2\pi)^6$, which originates from our convention of the normalization, $\langle \boldsymbol{p}_a'\boldsymbol{p}_b'\boldsymbol{p}_c' \mid \boldsymbol{p}_a\boldsymbol{p}_b\boldsymbol{p}_c\rangle=\delta(\boldsymbol{q}_a)\delta(\boldsymbol{q}_b)\delta(\boldsymbol{q}_c)$. See Refs. [24,47] for more details.

Although a local regulator depending on $\boldsymbol{q}_i$ is adopted in Ref. [24], alternatively we employ a nonlocal regulator,

$$u_\nu(k,K,\Lambda_0)=\exp\left[-\left(\frac{k^2+K^2}{2\Lambda_0^2}\right)^\nu\right], \tag{A8}$$

which is consistent with that for the two-body N^{3}LO potential with $\Lambda_0=500$ MeV and $\nu=2$. The Jacobi momenta $\boldsymbol{k}$ and $\boldsymbol{K}$ are defined by

$$\boldsymbol{k}=\frac{1}{\sqrt{2}}(\boldsymbol{p}_a-\boldsymbol{p}_b),\quad \boldsymbol{K}=\sqrt{\frac{2}{3}}\left[\frac{1}{2}(\boldsymbol{p}_a+\boldsymbol{p}_b)-\boldsymbol{p}_c\right]. \tag{A9}$$

Thus we regularize $w_{3N}^{(2\pi;c_\mu)}$ as

$$w_{3N}^{(2\pi;c_\mu)}(\boldsymbol{q}_b,\boldsymbol{q}_c)\to u_\nu(k',K',\Lambda_0)w_{3N}^{(2\pi;c_\mu)}(\boldsymbol{q}_b,\boldsymbol{q}_c)u_\nu(k,K,\Lambda_0), \tag{A10}$$

and we express it in terms of k, k', K, K', $\cos\theta_1$, $\cos\theta_2$, and $\cos\theta_3$, where the prime stands for the Jacobi momenta in the final channel and θ_1, θ_2, and θ_3 are the angles between $\boldsymbol{K}$ and $\boldsymbol{K}'$, $\boldsymbol{k}$ and $\boldsymbol{k}'$, and $\boldsymbol{K}-\boldsymbol{K}'$ and $\boldsymbol{k}-\boldsymbol{k}'$, respectively. Successively, we perform the triple-fold multipole expansion for these angles. As a result, we obtain the regularized 3BMEs of each operator as

$$\begin{aligned}\langle\bar\kappa';JT|W_{3N}^{(2\pi;c_1)}|\bar\kappa;JT\rangle=&\,3c_1m_\pi^2S_{\bar\kappa\bar\kappa'}^{JT}\begin{Bmatrix}\bar S_{12}&\bar S_{12}'&1\\ \frac12&\frac12&\frac12\end{Bmatrix}\begin{Bmatrix}\bar T_{12}&\bar T_{12}'&1\\ \frac12&\frac12&\frac12\end{Bmatrix}\sum_{\substack{\lambda_b\lambda_c\\ \lambda_b'\lambda_b''}}\sum_{\substack{\lambda_1\lambda_2\lambda_3\\ \lambda_3'\lambda_3''}}\sum_{l_1}(-1)^{\lambda_b+l_1+1}\hat l_1^2\\ &\times I^{\nu\lambda_b\lambda_c\lambda_b'\lambda_b''\lambda_1\lambda_2\lambda_3\lambda_3'\lambda_3''}_{\bar\kappa\bar\kappa' L_b=2,L_c=2,L_b'=1,L_c'=1}(\Lambda_0)X^{\lambda_b\lambda_c\lambda_b'\lambda_b''\lambda_1\lambda_2\lambda_3\lambda_3'\lambda_3''}_{\bar\kappa\bar\kappa' J,L_0=1,L_b'=1,L_c'=1,l_0=\lambda_b,l_1},\end{aligned} \tag{A11}$$

$$\begin{aligned}\langle\bar\kappa';JT|W_{3N}^{(2\pi;c_3)}|\bar\kappa;JT\rangle=&\,\frac{\sqrt3}{2}c_3S_{\bar\kappa\bar\kappa'}^{JT}\begin{Bmatrix}\bar S_{12}&\bar S_{12}'&1\\ \frac12&\frac12&\frac12\end{Bmatrix}\begin{Bmatrix}\bar T_{12}&\bar T_{12}'&1\\ \frac12&\frac12&\frac12\end{Bmatrix}\sum_{L_bL_c}\sum_{\substack{\lambda_b\lambda_c\\ \lambda_b'\lambda_b''}}\sum_{\substack{\lambda_1\lambda_2\lambda_3\\ \lambda_3'\lambda_3''}}\sum_{l_0l_1}\hat L_b\hat L_c\hat l_0^2\hat l_1^2(1010|L_b0)\\ &\times(1010|L_c0)\begin{Bmatrix}L_b-\lambda_b&\lambda_b&L_b\\ 1&1&l_0\end{Bmatrix}\begin{Bmatrix}l_0&l_1&1\\ L_c&1&\lambda_b\end{Bmatrix}I^{\nu\lambda_b\lambda_c\lambda_b'\lambda_b''\lambda_1\lambda_2\lambda_3\lambda_3'\lambda_3''}_{\bar\kappa\bar\kappa' L_bL_c,L_b'=L_b,L_c'=L_c}(\Lambda_0)\\ &\times X^{\lambda_b\lambda_c\lambda_b'\lambda_b''\lambda_1\lambda_2\lambda_3\lambda_3'\lambda_3''}_{\bar\kappa\bar\kappa' J,L_0=1,L_b'=L_b,L_c'=L_c,l_0l_1},\end{aligned} \tag{A12}$$

$$\begin{aligned}\langle\bar\kappa';JT|W_{3N}^{(2\pi;c_4)}|\bar\kappa;JT\rangle=&\,9\sqrt3c_4(-)^{l_{12}'+1}S_{\bar\kappa\bar\kappa'}^{JT}\begin{Bmatrix}\frac12&\frac12&\bar T_{12}'\\ \frac12&\frac12&\bar T_{12}\\ 1&1&1\end{Bmatrix}\sum_{\substack{L_0\\ L_bL_c}}\sum_{\substack{\lambda_b\lambda_c\\ \lambda_b'\lambda_b''}}\sum_{\substack{\lambda_1\lambda_2\lambda_3\\ \lambda_3'\lambda_3''}}\sum_{l_0l_1}\hat L_0^2\hat L_b\hat L_c\hat l_0^2\hat l_1^2(1010|L_b0)(1010|L_c0)\\ &\times\begin{Bmatrix}L_0&L_b&1\\ 1&1&1\end{Bmatrix}\begin{Bmatrix}L_b-\lambda_b&\lambda_b&L_b\\ 1&L_0&l_0\end{Bmatrix}\begin{Bmatrix}l_0&l_1&1\\ L_c&1&\lambda_b\end{Bmatrix}\begin{Bmatrix}\frac12&\frac12&\bar S_{12}'\\ \frac12&\frac12&\bar S_{12}\\ 1&1&L_0\end{Bmatrix}I^{\nu\lambda_b\lambda_c\lambda_b'\lambda_b''\lambda_1\lambda_2\lambda_3\lambda_3'\lambda_3''}_{\bar\kappa\bar\kappa' L_bL_c,L_b'=L_b,L_c'=L_c}(\Lambda_0)\\ &\times X^{\lambda_b\lambda_c\lambda_b'\lambda_b''\lambda_1\lambda_2\lambda_3\lambda_3'\lambda_3''}_{\bar\kappa\bar\kappa' J,L_0L_b'=L_b,L_c'=L_c,l_0l_1},\end{aligned} \tag{A13}$$

where, in general, $\hat{x} = \sqrt{2x+1}$. The coefficients in Eqs. (A11)–(A13) are defined as

$$S^{JT}_{\bar{\kappa}\bar{\kappa}'} = \left[\frac{g_A}{(\pi f_\pi)^2}\right]^2 i^{\bar{l}_{12}+\bar{l}'_{12}+\bar{l}+\bar{l}'}(-)^{\bar{S}_{12}+\bar{I}'_{12}-\bar{I}+\mathcal{I}+\bar{T}_{12}+\bar{T}'_{12}+T+\frac{1}{2}}\hat{\bar{S}}_{12}\hat{\bar{S}}'_{12}\hat{\bar{I}}_{12}\hat{\bar{I}}'_{12}\hat{\bar{I}}\hat{\bar{I}}'\hat{\bar{T}}_{12}\hat{\bar{T}}'_{12}\begin{Bmatrix}\bar{T}_{12} & \bar{T}'_{12} & 1\\ \frac{1}{2} & \frac{1}{2} & T\end{Bmatrix}, \tag{A14}$$

$$\begin{aligned}
I^{\nu\lambda_b\lambda_c\lambda'_b\lambda''_b\lambda_1\lambda_2\lambda_3\lambda'_3\lambda''_3}_{\bar{\kappa}\bar{\kappa}'L_bL_cL'_bL'_c}(\Lambda_0) &= 3^{-\frac{\lambda_b}{2}}(-1)^{\lambda_b+\lambda_c+\lambda'_b+\lambda''_b+\lambda_1+\lambda_2+\lambda_3+\lambda'_3+\lambda''_3}\widehat{L'_b-\lambda_b}\ \widehat{L'_c-\lambda_c}\ \widehat{L'_b-\lambda_b-\lambda'_b}\ \widehat{\lambda_b-\lambda''_b}\ \widehat{\lambda_3-\lambda'_3}\ \widehat{\lambda_3-\lambda''_3}\\
&\times\left[C^{2L'_b+1}_{2\lambda_b}C^{2L'_c+1}_{2\lambda_c}C^{2(L'_b-\lambda_b)+1}_{2\lambda'_b}C^{2\lambda_b+1}_{2\lambda''_b}C^{2\lambda_3+1}_{2\lambda'_3}C^{2\lambda_3+1}_{2\lambda''_3}\right]^{\frac{1}{2}}\int\int\int\int dkdKdk'dK'\,f^{(L_bL_c)}_{\lambda_1\lambda_2\lambda_3}(k,k',K,K')\\
&\times k^{L'_b-\lambda_b-\lambda'_b+\lambda_3-\lambda'_3+1}K^{L'_c-\lambda_c+\lambda_b-\lambda''_b+\lambda_3-\lambda''_3+1}\\
&\times k'^{\lambda'_b+\lambda'_3+1}K'^{\lambda_c+\lambda''_b+\lambda''_3+1}P_{\bar{n}_{12}\bar{l}_{12}}(k)P_{\bar{n}\bar{l}}(K)P_{\bar{n}'_{12}\bar{l}'_{12}}(k')P_{\bar{n}'\bar{l}'}(K')u_\nu(k,K,\Lambda_0)u_\nu(k',K',\Lambda_0),
\end{aligned} \tag{A15}$$

$$\begin{aligned}
X^{\lambda_b\lambda_c\lambda'_b\lambda''_b\lambda_1\lambda_2\lambda_3\lambda'_3\lambda''_3}_{\bar{\kappa}\bar{\kappa}'JL_0L'_bL'_cl_0l_1} &= \sum_{l_2l_3}\sum_{\substack{\lambda\lambda'\\ \Lambda\Lambda'}}\sum_{L_1L_2L_3}(-1)^{L_1+L_2+L_3}\hat{l}_2\hat{l}_3\hat{\lambda}\hat{\lambda}'\hat{\Lambda}\hat{\Lambda}'\hat{L}_1^2\hat{L}_2^2\hat{L}_3^2(L'_c-\lambda_c,0,\lambda_b-\lambda''_b,0|l_20)(\lambda_c0\lambda''_b0|l_30)\\
&\times(L'_b-\lambda_b-\lambda'_b,0\lambda0|\bar{l}_{12}0)(\lambda'_b0\lambda'0|\bar{l}'_{12}0)(l_20\Lambda0|\bar{l}0)(l_30\Lambda'0|\bar{l}'0)(\lambda_20,\lambda_3-\lambda'_3,0|\lambda0)(\lambda_20\lambda'_30|\lambda'0)\\
&\times(\lambda_10,\lambda_3-\lambda''_3,0|\Lambda0)(\lambda_10\lambda''_30|\Lambda'0)\begin{Bmatrix}\lambda_3-\lambda'_3 & \lambda'_3 & \lambda_3\\ \lambda' & \lambda & \lambda_2\end{Bmatrix}\begin{Bmatrix}\lambda_3-\lambda''_3 & \lambda''_3 & \lambda_3\\ \Lambda' & \Lambda & \lambda_1\end{Bmatrix}\\
&\times\begin{Bmatrix}\bar{I}_{12} & \bar{I}'_{12} & L_1\\ \bar{I}' & \bar{I} & J\end{Bmatrix}\begin{Bmatrix}L_0 & L'_b-\lambda_b & l_0\\ \lambda_3 & L_1 & L_2\end{Bmatrix}\begin{Bmatrix}1 & l_1 & l_0\\ \lambda_3 & L_1 & L_3\end{Bmatrix}\\
&\times\begin{Bmatrix}\lambda_b-\lambda''_b & \lambda''_b & \lambda_b\\ L'_c-\lambda_c & \lambda_c & L'_c\\ l_2 & l_3 & l_1\end{Bmatrix}\begin{Bmatrix}\bar{S}'_{12} & \bar{l}'_{12} & \bar{I}'_{12}\\ \bar{S}_{12} & \bar{l}_{12} & \bar{I}_{12}\\ L_0 & L_2 & L_1\end{Bmatrix}\begin{Bmatrix}\frac{1}{2} & \bar{l}' & \bar{I}'\\ \frac{1}{2} & \bar{l} & \bar{I}\\ 1 & L_3 & L_1\end{Bmatrix}\\
&\times\begin{Bmatrix}L'_b-\lambda_b-\lambda'_b & \lambda'_b & L'_b-\lambda_b\\ \lambda & \lambda' & \lambda_3\\ \bar{l}_{12} & \bar{l}'_{12} & L_2\end{Bmatrix}\begin{Bmatrix}l_2 & l_3 & l_1\\ \Lambda & \Lambda' & \lambda_3\\ \bar{l} & \bar{l}' & L_3\end{Bmatrix},
\end{aligned} \tag{A16}$$

where C^p_q and P_{nl} are the binomial coefficient $C^p_q = p!/[(p-q)!q!]$ and the momentum-space HO wave functions, respectively. Note that the phase of P_{nl} is chosen to be consistent with a convention employed in the Fortran code [43]. The multipole-expansion function $f^{(L_bL_c)}_{\lambda_1\lambda_2\lambda_3}$ is defined as

$$\begin{aligned}
f^{(L_bL_c)}_{\lambda_1\lambda_2\lambda_3}(k,k',K,K') &= \frac{\hat{\lambda}_1^2\hat{\lambda}_2^2\hat{\lambda}_3^2}{8}\int_{-1}^{1}\int_{-1}^{1}\int_{-1}^{1}dw_1dw_2dw_3P_{\lambda_1}(w_1)P_{\lambda_2}(w_2)P_{\lambda_3}(w_3)\\
&\times(|\boldsymbol{k}-\boldsymbol{k}'||\boldsymbol{K}-\boldsymbol{K}'|)^{-\lambda_3}\frac{2^{-\frac{L_b}{2}}\left(\frac{2}{3}\right)^{\frac{L_c}{2}}q_b^{2-L_b}q_c^{2-L_c}}{\left(q_b^2+m_\pi^2\right)\left(q_c^2+m_\pi^2\right)},
\end{aligned} \tag{A17}$$

where P_{λ_m} is the Legendre polynomial with $w_m = \cos\theta_m$ ($m = 1$, 2, or 3).

[1] T. T. S. Kuo and G. E. Brown, Nucl. Phys. **85**, 40 (1966).
[2] T. Hamada and I. D. Johnston, Nucl. Phys. **34**, 382 (1962).
[3] M. Hjorth-Jensen, T. T. S. Kuo, and E. Osnes, Phys. Rep. **261**, 125 (1995).
[4] L. Coraggio, A. Covello, A. Gargano, N. Itaco, and T. T. S. Kuo, Prog. Part. Nucl. Phys. **62**, 135 (2009).
[5] *The Nucleon-nucleon Interaction and the Nuclear Many-body Problem: Selected Papers of Gerald E. Brown and T. T. S. Kuo*, edited by G. E. Brown, T. T. S. Kuo, J. W. Holt, and S. Lee (World Scientific, Singapore, 2010).
[6] T. T. S. Kuo and E. Osnes, *Lecture Notes in Physics* (Springer-Verlag, Berlin, 1990), Vol. 364.
[7] K. Suzuki and S. Y. Lee, Prog. Theor. Phys. **64**, 2091 (1980).
[8] S. K. Bogner, H. Hergert, J. D. Holt, A. Schwenk, S. Binder, A. Calci, J. Langhammer, and R. Roth, Phys. Rev. Lett. **113**, 142501 (2014).
[9] H. Hergert, S. K. Bogner, T. D. Morris, A. Schwenk, and K. Tsukiyama, Phys. Rep. **621**, 165 (2016).
[10] L. Coraggio, A. Covello, A. Gargano, N. Itaco, and T. T. S. Kuo, Ann. Phys. (NY) **327**, 2125 (2012).
[11] P. Navrátil and E. Caurier, Phys. Rev. C **69**, 014311 (2004).
[12] P. Navrátil, V. G. Gueorguiev, J. P. Vary, W. E. Ormand, and A. Nogga, Phys. Rev. Lett. **99**, 042501 (2007).
[13] D. R. Entem and R. Machleidt, Phys. Rev. C **66**, 014002 (2002).
[14] P. J. Ellis and E. Osnes, Rev. Mod. Phys. **49**, 777 (1977).

[15] A. Polls, H. Müther, A. Faessler, T. T. S. Kuo, and E. Osnes, Nucl. Phys. A **401**, 124 (1983).
[16] R. Machleidt and D. R. Entem, Phys. Rep. **503**, 1 (2011).
[17] S. C. Pieper and R. B. Wiringa, Annu. Rev. Nucl. Part. Sci. **51**, 53 (2001).
[18] S. C. Pieper, Nucl. Phys. A **751**, 516 (2005).
[19] P. Maris, J. P. Vary, and P. Navrátil, Phys. Rev. C **87**, 014327 (2013).
[20] T. Otsuka, T. Suzuki, J. D. Holt, A. Schwenk, and Y. Akaishi, Phys. Rev. Lett. **105**, 032501 (2010).
[21] J. D. Holt, J. Menéndez, and A. Schwenk, Phys. Rev. Lett. **110**, 022502 (2013).
[22] J. D. Holt, J. Menéndez, J. Simonis, and A. Schwenk, Phys. Rev. C **90**, 024312 (2014).
[23] J. Simonis, K. Hebeler, J. D. Holt, J. Menéndez, and A. Schwenk, Phys. Rev. C **93**, 011302 (2016).
[24] P. Navrátil, Few-Body Syst. **41**, 117 (2007).
[25] T. T. S. Kuo, S. Y. Lee, and K. F. Ratcliff, Nucl. Phys. A **176**, 65 (1971).
[26] G. A. Baker and J. L. Gammel, *The Padé Approximant in Theoretical Physics*, Vol. 71 of *Mathematics in Science and Engineering* (Academic Press, New York, 1970).
[27] N. Ayoub and H. A. Mavromatis, Nucl. Phys. A **323**, 125 (1979).
[28] H. M. Hoffmann, Y. Starkand, and M. W. Kirson, Nucl. Phys. A **266**, 138 (1976).
[29] E. Caurier, G. Martínez-Pinedo, F. Nowacki, A. Poves, and A. P. Zuker, Rev. Mod. Phys. **77**, 427 (2005).
[30] M. Hjorth-Jensen, M. P. Lombardo, and U. van Kolck, eds., *Lecture Notes in Physics* (Springer, Germany, 2017), Vol. 936.
[31] See Supplemental Material at http://link.aps.org/supplemental/10.1103/PhysRevC.98.044305 for the list of two-body matrix elements of the shell-model Hamiltonian $H_{\rm eff}$.
[32] Data extracted by using the NNDC On-line Data Service from the ENSDF database, file revised as of March 6, 2018, https://www.nndc.bnl.gov/ensdf.
[33] A. P. Zuker, Phys. Rev. Lett. **90**, 042502 (2003).
[34] A. Schwenk and A. P. Zuker, Phys. Rev. C **74**, 061302 (2006).
[35] N. Tsunoda, T. Otsuka, N. Shimizu, M. Hjorth-Jensen, K. Takayanagi, and T. Suzuki, Phys. Rev. C **95**, 021304 (2017).
[36] S. K. Bogner, A. Schwenk, R. J. Furnstahl, and A. Nogga, Nucl. Phys. A **763**, 59 (2005).
[37] R. Roth, A. Calci, J. Langhammer, and S. Binder, Phys. Rev. C **90**, 024325 (2014).
[38] I. Talmi, Helv. Phys. Acta **25**, 185 (1952).
[39] T. A. Brody and M. Moshinsky, *Tables of Transformation Brackets* (Monografias del Instituto de Fisica, Mexico, 1960).
[40] M. Moshinsky and T. A. Brody, Rev. Mex. Fís. **9**, 181 (1960).
[41] L. Trlifaj, Phys. Rev. C **5**, 1534 (1972).
[42] B. Buck and A. C. Merchant, Nucl. Phys. A **600**, 387 (1996).
[43] G. P. Kamuntavičius, R. K. Kalinauskas, B. R. Barrett, S. Mickevičius, and D. Germanas, Nucl. Phys. A **695**, 191 (2001).
[44] P. Navrátil, B. R. Barrett, and W. Glöckle, Phys. Rev. C **59**, 611 (1999).
[45] P. Navrátil, G. P. Kamuntavičius, and B. R. Barrett, Phys. Rev. C **61**, 044001 (2000).
[46] E. Epelbaum, Prog. Part. Nucl. Phys. **57**, 654 (2006).
[47] S. A. Coon and W. Glöckle, Phys. Rev. C **23**, 1790 (1981).